DEVELOPMENTAL DYNAMICS 237:3410–3416, 2008

Generation and Expression of a *Hoxa11eGFP* Targeted Allele in Mice

Lisa T. Nelson,[1] Sabita Rakshit,[1] Hanshi Sun,[1] and Deneen M. Wellik[1,2]*

***Hox* genes are crucial for body axis specification during embryonic development. *Hoxa11* plays a role in anteroposterior patterning of the axial skeleton, development of the urogenital tract of both sexes, and proximodistal patterning of the limbs. *Hoxa11* expression is also observed in the neural tube. Herein, we report the generation of a *Hoxa11eGFP* targeted knock-in allele in mice in which *eGFP* replaces the first coding exon of *Hoxa11* as an in-frame fusion. This allele closely recapitulates the reported mRNA expression patterns for *Hoxa11*. Hoxa11eGFP can be visualized in the tail, neural tube, limbs, kidneys, and reproductive tract of both sexes. Additionally, homozygous mutants recapitulate reported phenotypes for *Hoxa11* loss of function mice, exhibiting loss of fertility in both males and females. This targeted mouse line will prove useful as a vital marker for Hoxa11 protein localization during control (heterozygous) or mutant organogenesis. *Developmental Dynamics 237:3410–3416, 2008.* © 2008 Wiley-Liss, Inc.**

Key words: Hoxa11; eGFP; targeted mutation

Accepted 2 September 2008

INTRODUCTION

Hox genes were first described in *Drosophila* and are homeodomain containing transcription factors that play a role in body axis specification during embryonic development (Wellik, 2007). In mammals, there are 39 *Hox* genes arranged in four clusters, A, B, C, and D, which have arisen through duplications of an ancestral cluster during evolution. Based on sequence similarity, these clusters can be aligned into 13 paralogous groups, with *Hox1* located most 3′ on the chromosome and *Hox13* most 5′. During development, the Hox genes are expressed colinearly along the primary body axis with 3′ genes expressed earlier and with more anterior limits, and more 5′ genes expressed later with increasingly posterior boundaries. Members of each paralogous group exhibit similar expression patterns along the anterioposterior (AP) axis and are functionally redundant in many developmental processes. (Condie and Capecchi, 1994; Davis et al., 1995; Horan et al., 1995; Fromental-Ramain et al., 1996; Warot et al., 1997; van den Akker et al., 2001; Wellik et al., 2002; Wellik and Capecchi, 2003; McIntyre et al., 2007).

In mice, expression patterns for *Hoxa11* mRNA have been previously reported. Faint expression is first detected at approximately E9.0 in the posterior tip of the embryo. By E10.5, expression in the tail has increased in intensity and expression is also observed in all four limb buds (Small and Potter, 1993). As limb bud morphogenesis proceeds, the mRNA expression pattern undergoes well documented, dynamic changes. The expression is concentrated in the distal limb bud until approximately E11 (Peichel et al., 1997), then becomes localized to the developing zeugopod region at subsequent stages (Haack and Gruss, 1993; Hsieh-Li et al., 1995). In the developing kidney, *Hoxa11* expression has been reported in the metanephric blastema before ureteric bud induction (Patterson et al., 2001), and later, expression is restricted to the nephrogenic mesenchyme during stages of branching

[1]Division of Molecular Medicine and Genetics, Department of Internal Medicine, University of Michigan Medical School, Ann Arbor, Michigan
[2]Department of Cell and Developmental Biology, University of Michigan Medical School, Ann Arbor, Michigan
Grant sponsor: NIH; Grant number: DK071929; Grant number: DK077045.
***Correspondence to: Deneen M. Wellik, University of Michigan Medical Center, 109 Zina Pitcher Place, 2053 BSRB, Ann Arbor, MI 48109-2200. E-mail: dwellik@umich.edu**

DOI 10.1002/dvdy.21756
Published online 15 October 2008 in Wiley InterScience (www.interscience.wiley.com).

morphogenesis (Patterson et al., 2001). In the adult reproductive system, *Hoxa11* expression has been documented in the uterus in females and in the vas deferens in males (Hsieh-Li et al., 1995).

Loss of function of *Hoxa11* in the developing embryo results in relatively mild malformations in the axial and appendicular skeleton and defects in the reproductive system of both males and females (Small and Potter, 1993; Hsieh-Li et al., 1995; Gendron et al., 1997; Wong et al., 2004). Mutants of both sexes are infertile (Hsieh-Li et al., 1995). Males exhibit transformation of the vas deferens to an epididymal fate, and the testis do not descend. Mutant females have apparently normal ovaries; however, the uterine environment is unable to support implantation (Hsieh-Li et al., 1995; Gendron et al., 1997; Wong et al., 2004). *Hoxa11* mutant mice have no detectable kidney phenotype (Hsieh-Li et al., 1995), but mutation of two or more *Hox11* group genes results in severe kidney defects (Davis et al., 1995; Patterson et al., 2001; Wellik et al., 2002).

We have generated a targeted *Hoxa11eGFP* knock-in allele in mice. The eGFP allows real-time visualization of Hoxa11 expression in the developing embryo as well as in the adult mouse. eGFP detection closely follows what has been reported for *Hoxa11* mRNA expression (Haack and Gruss, 1993; Small and Potter, 1993; Hsieh-Li et al., 1995; Peichel et al., 1997; Patterson et al., 2001), thus it serves as an useful marker for Hoxa11 protein localization in vivo.

RESULTS AND DISCUSSION

Crosses between *Hoxa11eGFP* heterozygotes produced offspring in normal Mendelian ratios. Breeding *Hoxa11eGFP* to homozygosity results in infertility in both sexes, which follows the previously reported *Hoxa11* mutant phenotype (Hsieh-Li et al., 1995). Additionally, generation of triple heterozygous mice (*Hoxa11eGFP* +/−; *Hoxc11* +/−; *Hoxd11* +/−) also results in infertility as previously reported (Wellik et al., 2002).

Whole-Mount Expression

Hoxa11eGFP localization is first observed at approximately embryonic day (E) 9.0, slightly later than the reported mRNA expression pattern. This is likely due to the time required for mRNA translation into protein and eGFP accumulation to detectable levels. At E9.5, Hoxa11eGFP localization is observed in the tip of the tail and faintly in the emerging forelimb bud (Fig. 1B). By E10.5, localization in the forelimb is more intense and restricted to the distal end of the bud. At this stage, Hoxa11eGFP is also localized in the emerging hindlimbs and in the neural tube and flank mesoderm from the mid-hindlimb region to the posterior tip of the tail (Fig. 1D). Fidelity of the Hoxa11eGFP detection is evident by comparison with the *Hoxa11* mRNA expression pattern observed in whole-mount embryos (compare Fig. 1C with 1D). After E11.5, fluorescence becomes restricted to a more proximal region of the developing limbs, and becomes less intense in the autopod (Fig. 1F,H,J,L). Detection in the tail peaks at E10.5 and decreases in intensity at later developmental stages (Fig. 1D,F,H,J,L). Hoxa11eGFP fluorescence can be detected in the tail, neural tube and limb buds in whole-mount animals through newborn stages (Fig. 1L and data not shown). Fluorescence is visible in fresh, fixed and cryopreserved tissues (see the Experimental Procedures section). No fluorescence is detected in wild-type embryos at the same settings used to detect eGFP (Fig. 1I and data not shown).

Limb Expression

Hoxa11eGFP localization in the limbs closely follows the dynamic patterns previously reported for mRNA expression (Haack and Gruss, 1993; Small and Potter, 1993; Hsieh-Li et al., 1995). Hoxa11eGFP is first detected in the emerging forelimb buds at E9.5 (Fig. 1B). By E10.5, strong fluorescence is noted in both the forelimb and hindlimb buds (Fig. 1D). At this stage, localization appears to be throughout most of the limb bud by whole-mount analysis (Fig. 1D); however, section analysis reveals that Hoxa11eGFP is localized uniformly in all mesenchymal cells of the distal limb bud, but in only a subset of cells proximally (Fig. 2A). Ubiquitous expression throughout the distal limb bud remains at E11.5, with a subset of cells in the proximal limb bud maintaining strong eGFP fluorescence (Fig. 2B). Hoxa11eGFP is excluded from the cells in the center of the proximal limb (Fig. 2B). Co-staining at this stage with antibodies to Sox9, a precartilaginous marker, reveals mutually exclusive expression with Sox9 in the central region of the limb bud. Only a small band of colocalization is observed toward the distal portion of Sox9 expression (Fig. 2B). By E12.5, Hoxa11eGFP becomes localized to the developing zeugopod region with lower levels of expression detected in the autopod (Fig. 2C). Hoxa11eGFP is observed in the distal zeugopod region at E13.5, and is detected more faintly in the interdigital region of the autopod (Fig. 2E). Co-staining with Sox9 at this stage allows the condensing cartilage to be visualized. Hoxa11eGFP and Sox9 appear to be co-expressed at the distal ends of the developing radius and ulna, but otherwise remain mutually exclusive (Fig. 2E). At later stages, Hoxa11eGFP is localized at the distal zeugopod, where it is detected surrounding the distal radius and ulna in perichondrial regions (Fig. 2E,F). Relatively faint localization in the interdigital mesenchyme of the autopod is observed at E12.5 (Fig. 2C). At E15.5 and beyond, Hoxa11eGFP expression in the autopod becomes restricted to cells surrounding the condensing digit cartilage (Fig. 2F and data not shown). Comparison of a wild-type control with a Hoxa11eGFP limb section at E13.5 shows the relative background levels for this allele (compare Fig. 2D with 2E, no green fluorescence is detected at similar settings in the absence of the Hoxa11eGFP allele).

Urogenital Expression

In the early developing kidney, Hoxa11eGFP can be detected throughout the condensing metanephric mesenchyme and is never observed in the ureteric bud or its derivatives (Fig. 3A,B). As tubulogenesis proceeds, Hoxa11eGFP becomes localized to the progenitor cells surrounding the branching ureter tips and less intensely in the mesenchyme surround-

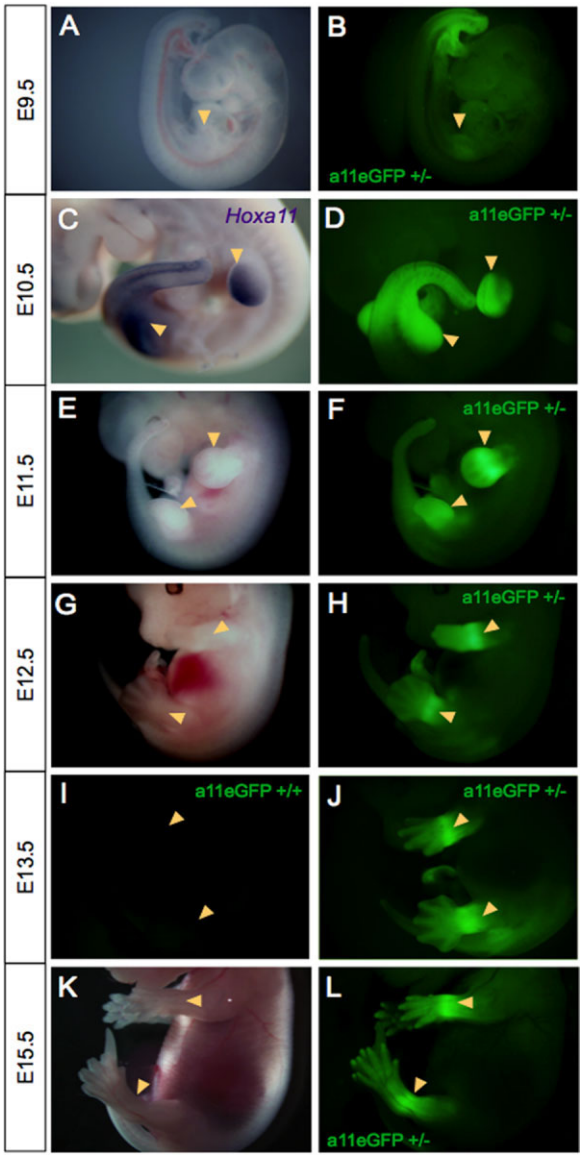

Fig. 1. Hoxa11eGFP fluorescence in whole-mount embryos. **A,B:** Embryonic day (E) 9.5 Hoxa11eGFP heterozygous embryos showing the brightfield view (A) and Hoxa11eGFP fluorescence (B). **C:** *Hoxa11* RNA in situ hybridization on an E10.5 wild-type embryo. **D:** An E10.5 Hoxa11eGFP heterozygous embryo showing eGFP fluorescence. **E,F:** E11.5 heterozygous Hoxa11eGFP embryo showing the brightfield view (E) and eGFP fluorescence (F). **G,H:** An E12.5 Hoxa11eGFP heterozygous embryo with the brightfield view (G) and eGFP fluorescence (H). **I:** An E13.5 wild-type embryo on the green fluorescence channel has no visible fluorescence at settings used for eGFP detection. **J:** An E13.5 Hoxa11eGFP heterozygous embryo showing eGFP fluorescence. **K,L:** An E15.5 Hoxa11eGFP heterozygous embryo with the brightfield view (K) and eGFP fluorescence (L). Arrowheads indicate regions of Hoxa11eGFP expression in the limbs in each panel.

Fig. 2. Hoxa11eGFP localization in cryosections through the forelimbs at various stages of development. **A:** A transverse section through a Hoxa11eGFP heterozygous forelimb at embryonic day (E) 10.5. **B:** Transverse section of a Hoxa11eGFP heterozygous forelimb at E11.5 co-stained with antibodies to Sox9, a prechrondrogenic marker. **C:** A transverse section through a Hoxa11eGFP heterozygous forelimb at E12.5. **D:** A transverse section through an E13.5 wild-type forelimb (no Hoxa11eGFP), using anti-Sox9 antibody staining (in red) and green channel fluorescence at the same settings as E. **E:** Transverse section through an Hoxa11eGFP heterozygous E13.5 forelimb co-stained with Sox9 in red. **F:** A transverse section through a Hoxa11eGFP heterozygous forelimb at E15.5. Scale bar = 500 microns in A–F.

Fig. 1.

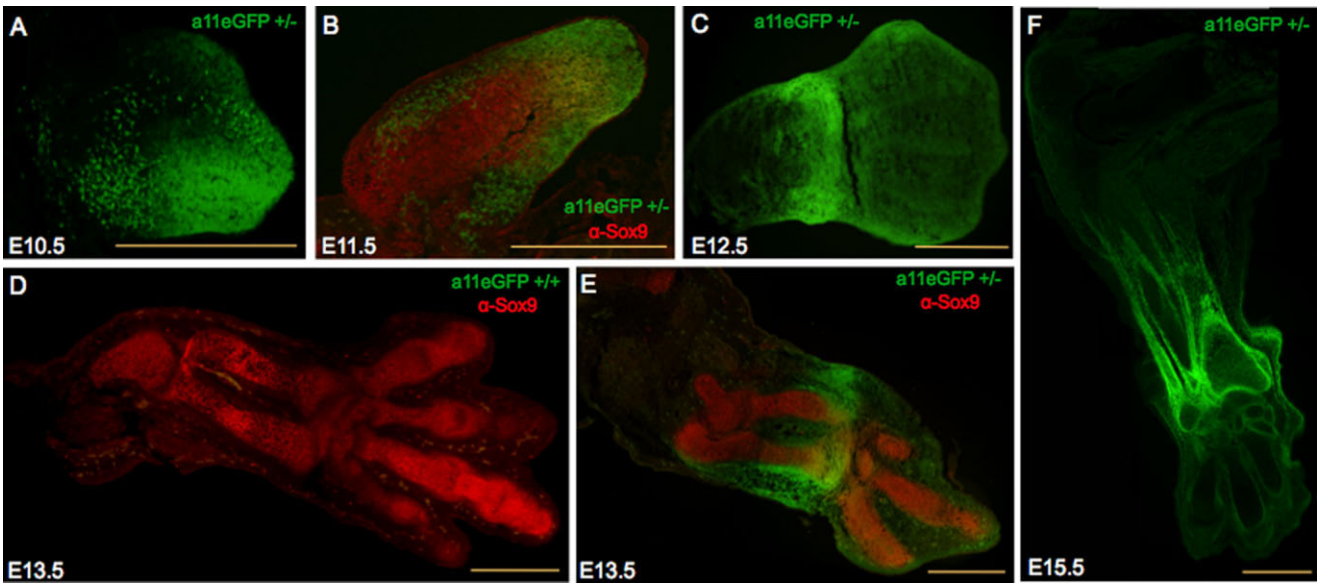

Fig. 2.

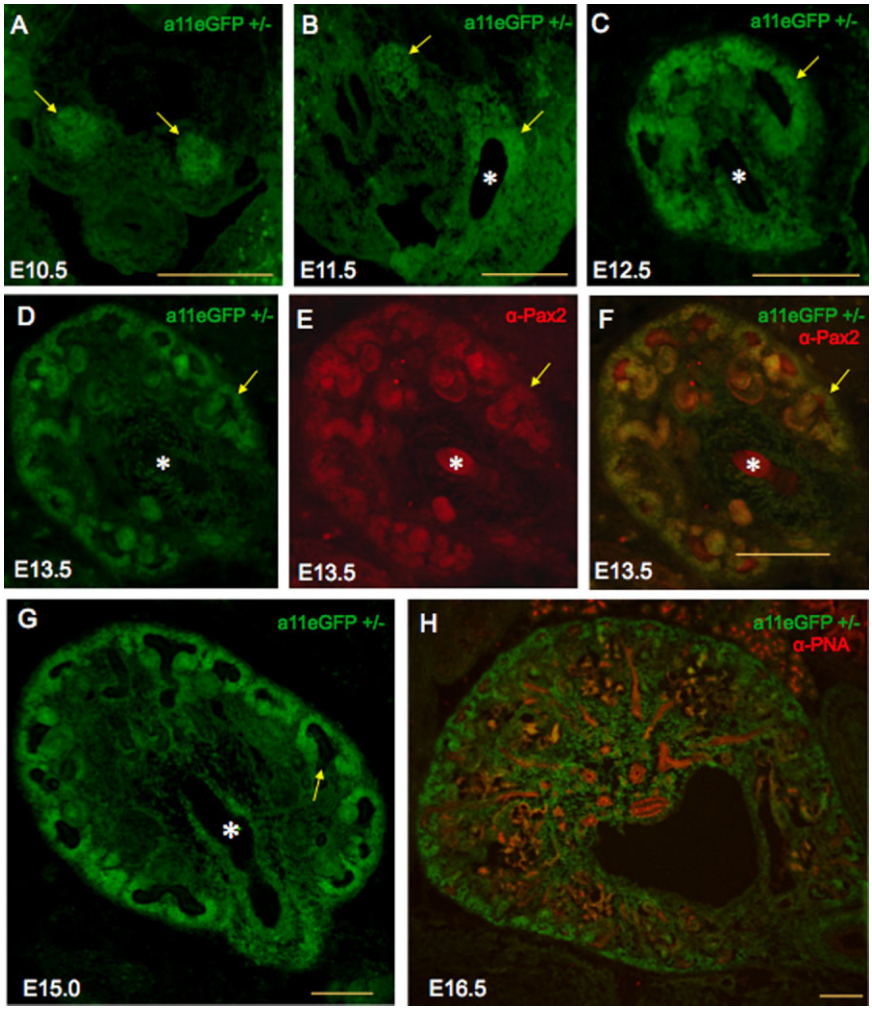

Fig. 3. Hoxa11eGFP fluorescence in transverse cryosections of the developing kidney. **A:** Hoxa11eGFP fluorescence in the condensing metanephric mesenchyme (arrows) of an embryonic day (E) 10.5 heterozygous embryo. **B:** Hoxa11eGFP heterozygous embryo at E11.5 with fluorescing metanephric mesenchyme (arrows) being invaded by the ureteric bud (white asterisk), which does not express Hoxa11eGFP. **C:** E12.5 kidney showing Hoxa11eGFP localized in the condensing nephrogenic mesenchyme (arrow) surrounding the ureteric bud (white asterisk). **D–F:** Hoxa11eGFP heterozygous kidney at E13.5 (D), co-stained with anti-Pax2 antibody (in red; E), and colocalizations of Hoxa11eGFP and Pax2 in this section (F). Colocalization of Hoxa11eGFP and Pax2 is observed in the condensing nephrogenic mesenchyme (arrow). The ureteric bud (white asterisk) and ureteric bud-derived elements show only Pax2 expression, and mesenchyme surrounding the ureter demonstrates only Hoxa11eGFP. **G:** In the E15.0 Hoxa11eGFP heterozygous kidney, fluorescence is detected in the condensing nephrogenic mesenchyme cells (arrow) and in mesenchyme surrounding the ureteric bud (white asterisk), which does not express the Hoxa11eGFP allele. **H:** PNA, which labels early collecting tubules, is largely nonoverlapping with Hoxa11eGFP at E16.5. Scale bars = 200 microns in A–H.

ing the ureter (Fig. 3C,D). Co-staining with antibodies to Pax2 at E13.5, a marker of nephrogenic mesenchyme and ureteric bud, demonstrates partially overlapping expression (Fig. 3D–F). Hoxa11eGFP and Pax2 are both expressed in the nephrogenic mesenchyme. Pax2 is exclusively expressed in the ureteric bud and its derivatives and Hoxa11eGFP is exclusively observed in the stromal mesenchyme surrounding the ureter. At E15.0, Hoxa11eGFP is observed in the nephrogenic mesenchyme and in mesenchymal cells surrounding the ureteric bud (Fig. 3G). Co-staining at E16.5 with peanut agglutinin (PNA), a collecting tubule marker, reveals largely exclusive expression with Hoxa11eGFP, although some co-staining in convoluted tubules is apparent (Fig. 3H). Localization of Hoxa11eGFP in the nephrogenic progenitor cells is maintained through approximately P8 and is not visible after this stage (data not shown).

In the female reproductive tract, Hoxa11eGFP is observed throughout the uterus but not in the ovaries. Localization in the uterus is established during the early differentiation of the tissue (Fig. 4A) and remains high throughout adulthood at all stages examined (Fig. 4C,E,G and data not shown). In males, Hoxa11eGFP is strongly expressed in the vas deferens from embryonic stages (Fig. 4B) through adulthood (Fig. 4D,F,H and data not shown).

Neural Tube Expression

From the earliest stages of *Hoxa11* expression, Hoxa11eGFP is observed in the neural tube (Fig. 1B). By E11.5 Hoxa11eGFP is localized to ventrolateral regions of the neural tube, correlating with areas of motor neuron differentiation (Fig. 5A). At E12.5 and E13.5 Hoxa11eGFP is observed in more dorsal and medial regions of the neural tube (Fig. 5B,C). Control embryos do not show GFP fluorescence at similar fluorescent settings (Fig. 5D and data not shown).

To summarize, we have generated a novel *Hoxa11eGFP* targeted allele in mice. This allele closely recapitulates documented *Hoxa11* mRNA expression patterns in the neural tube, limbs, and urogenital system, confirming that it is a faithful reporter of *Hoxa11* expression. This mouse line will be useful for studies of the dynamic Hoxa11 localization patterns during both control (heterozygous) and mutant development. Furthermore, the allele is stable in fresh as well as fixed tissues, and therefore will be a valuable reagent for vital studies.

EXPERIMENTAL PROCEDURES

Generation of the *Hoxa11eGFP* Allele in Mice

BAC clone RP23-20F21 that spans the entire *HoxA* complex was identified by screening the RPCI-23 C57Bl/6 library (Osoegawa et al., 2000). A total of 10 kb of genomic sequences including coding sequence for Hoxa11, in-

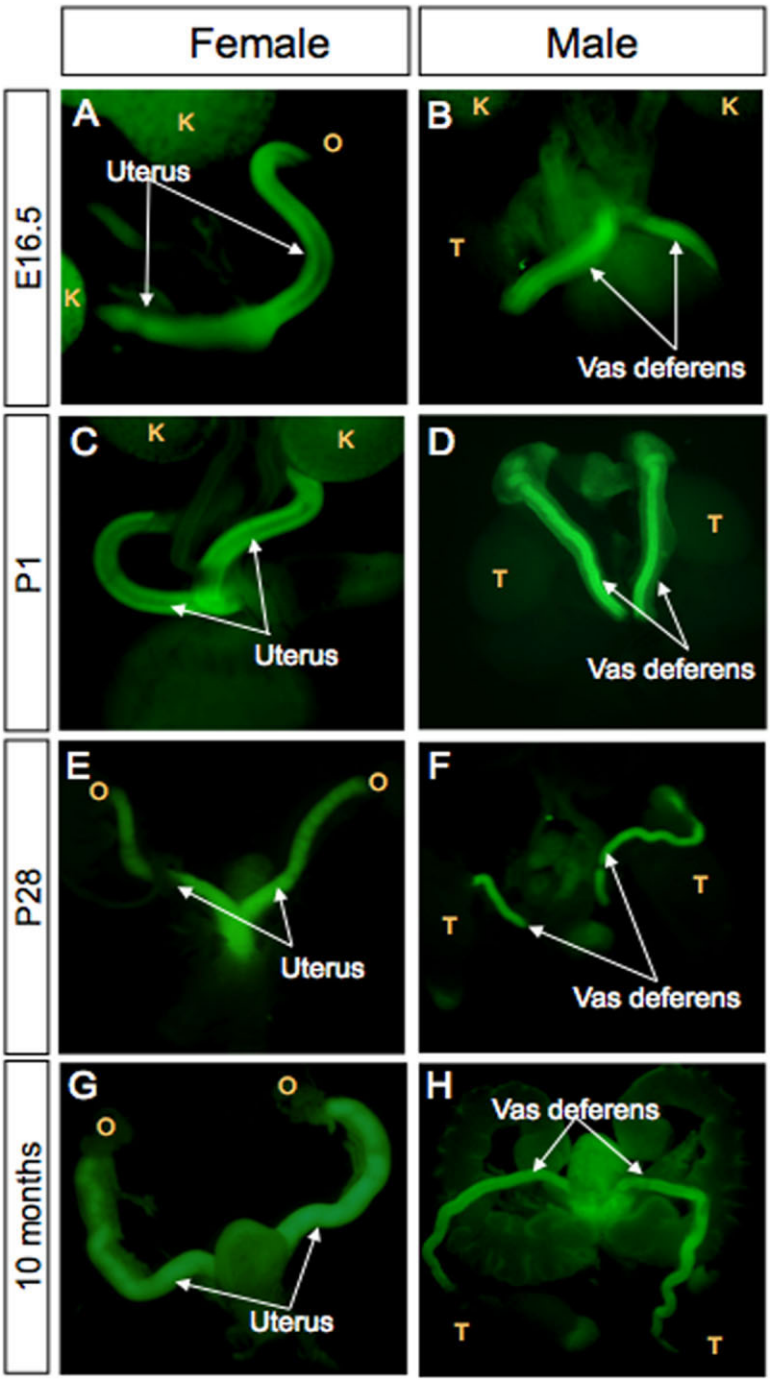

Fig. 4.

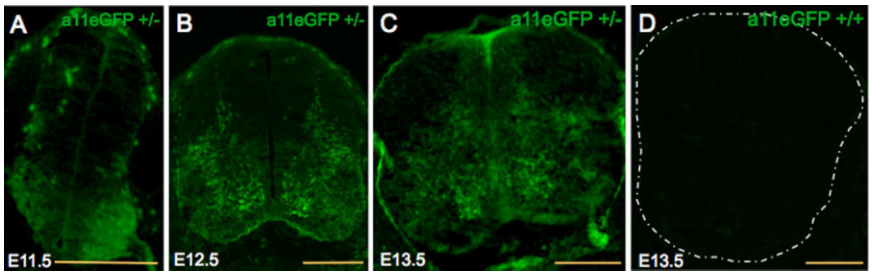

Fig. 5.

cluding 4.7 kb upstream of exon 1 and 0.7 kb downstream of exon 2 was subcloned using recombineering technology to an ASCL vector (Muyrers et al., 1999, 2004; McIntyre et al., 2007). An eGFP fluorescent fusion construct (eGFP, Clontech) was exchanged as an in-frame fusion 18 base pairs downstream of the start site in exon 1 of Hoxa11; this recombination event resulted in removal of most of exon 1. The eGFP fusion protein is followed by a SV40 poly-A strong stop signal, creating a null allele, which expresses eGFP in place of Hoxa11. Following the stop signal, there is a *tACE-Cre-Neo*^{r} (ACN) construct in the opposite orientation (Bunting et al., 1999). The *Neo*^{r} allows for selection of the embryonic stem (ES) cells after electroporation. The *tACE-Cre* drives expression of Cre from the testes-specific ACE promoter (Langford et al., 1991) and allows removal of the *Cre* and *Neo*^{r} sequences from the targeted locus during chimeric passage to germ line. The *Cre* coding sequence contains the SV40 small antigen intron which prevents leaky expression before germ-line transmission (Bunting et al., 1999). The ACN cassette is flanked by *LoxP* sites, allowing Cre-mediated excision of the cassette. TK was inserted 5′ to the genomic flanking sequence to provide positive selection and decrease random transgenic insertions of the targeting vector into nonhomologous regions. (Fig. 1A shows a schematic of the targeting vector.)

The Hoxa11eGFP targeting vector was electroporated into R1 ES cells

Fig. 4. Hoxa11eGFP fluorescence in heterozygous reproductive tracts from both sexes. **A,C,E,G:** Dissected female reproductive tracts at embryonic day (E) 16.5 (A), P1 (C), P28 (E), and 10 months (G). Hoxa11eGFP is observed in the developing uterus (arrows) and is excluded from the ovaries. **B,D,F,H:** Dissected male reproductive tracts at E16.5 (B), P1 (D), P28 (F), and 10 months (H). Intense Hoxa11eGFP localization is observed in the vas deferens (arrows). K, kidney; O, ovary; T, testis.

Fig. 5. Hoxa11eGFP fluorescence in the neural tube. **A–C:** Transverse cryosections through the sacral region of the neural tube of *Hoxa11eGFP* heterozygous embryos at embryonic day (E) 11.5 (A), E12.5 (B), and E13.5 (C). **D:** Transverse cryosection through the sacral region of the neural tube of a wild-type embryo at E13.5 photographed using the same fluorescence settings as for C. Scale bar = 200 microns in A–D.

Developmental Dynamics

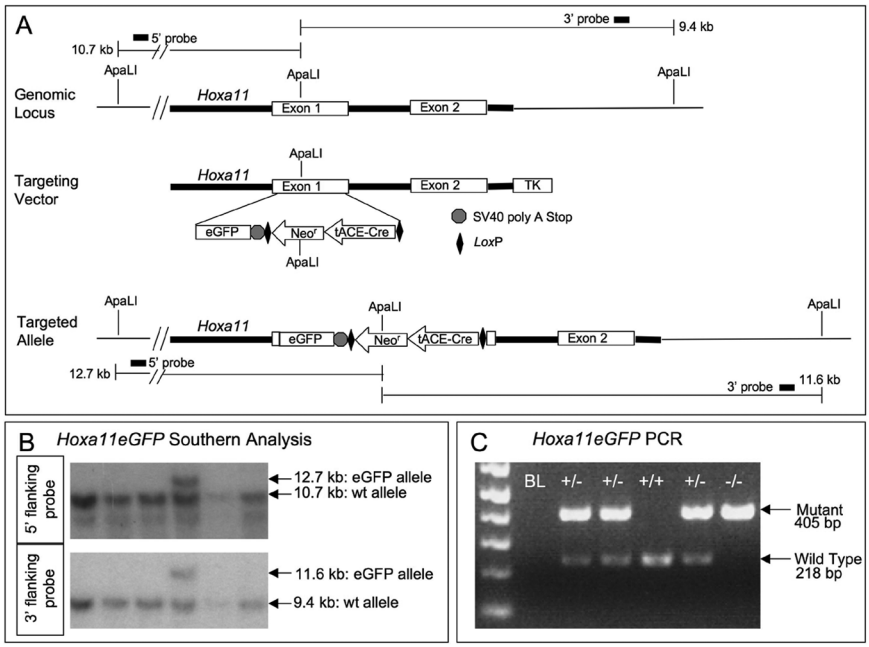

Fig. 6. Generation of *Hoxa11eGFP* targeted allele in mice. **A:** Schematic of the *Hoxa11* genomic locus, Hoxa11eGFP targeting vector and *Hoxa11eGFP* allele. Exon 1 of *Hoxa11* is replaced by *eGFP* followed by an SV40 T-antigen stop sequence and an ACN cassette in reverse orientation flanked by *LoxP* sites. A TK cassette is 5′ to the *Hoxa11* genomic flanking sequence. *Apa*LI restriction sites are shown for the wild-type allele as well as the Hoxa11eGFP targeted allele, and the sizes generated upon digest (used for Southern analysis). **B:** Southern analyses of *Hoxa11eGFP* targeted embryonic stem (ES) cells. Genomic DNA extracted from ES cells was digested with *Apa*LI and hybridized with either a 813-bp 5′ flanking probe or a 621-bp 3′ flanking probe. The 5′ probe detected 10.7- and 12.7-kb bands for wild-type and mutant alleles, respectively. The 3′ probe detected 9.4- and 11.6-kb bands for wild-type and mutant alleles, respectively. **C:** Polymerase chain reaction genotyping of *Hoxa11eGFP* mice. The bottom 218-bp band is the wild-type allele, and the top 405-bp band is the mutant *Hoxa11eGFP* allele (further details in the Experimental Procedures section).

(Nagy et al., 1993), and double selection was performed with G418 and FIAU (Mansour et al., 1988). Surviving clones were analyzed by Southern analysis to identify homologous recombinants using a 5′ flanking probe, a 3′ flanking probe and a *Neo*^{r} probe with ApaL1 digested DNA (Fig. 6B and data not shown). The 813-bp 5′ probe was generated using primers 5′-GTA TTT GAA TTC GAT GCC GAA CTG AGG CCA ATG GTT GT-3′ and 5′-AGC GTG TCT AGA GCT CTG CAG CAG AGC CGG ATA GAA AC-3′, and the 621-bp 3′ probe generated using primers 5′-CTC CTT TTG AAT TCG GAA TAG TCA GCG CTC TTG GGA CCC ACT-3′ and 5′-GCA CTC TGT CTA GAA GAG GAC ACA GGG AAG CTG ACC AGG TAG-3′, that were randomly labeled with ^{32}P-dCTP. Two positive clones were identified and injected into blastocysts. Twelve high-percentage, agouti chimeric founder males were generated and several transmitted the allele, all of which resulted in the removal of the ACN cassette. Polymerase chain reaction (PCR) analysis of tail DNA confirmed germ-line transmission of the allele and deletion of the ACN cassette (Fig. 6C). Three founder lines were then back-crossed to C57Bl/6 mice. All founder lines were found to be indistinguishable in phenotype.

Genotyping was performed by PCR using either tail or yolk sac DNA. The following primers were used to detect a 218-bp band for the wild-type allele, and a 405-bp band for the eGFP allele: Forward: 5′-CTA CTT CAC GGA TCC GCT TCA-3′, Reverse: 5′-GGT TGG AGG AGT AGG AGT ATG-3′, and eGFP reverse: 5′-ATG GTG CGC TCC TGG ACG TAG CCT T-3′ (Fig. 6C).

Embryo Collection, IHC Experiments and Image Acquisition

Embryos were collected at various stages of gestation for analyses. After dissection in PBS, they were fixed in formalin or 4% paraformaldehyde. Whole-mount images were taken on the Olympus SZX9 florescent dissecting microscope with an Olympus DP70 camera or the Leica MXFL III stereo fluorescent microscope with a Sony DKC5000 video-to-digital camera. After fixation, animals were equilibrated in 15% and then 30% sucrose, then embedded in Tissue-Tek O.C.T. Compound embedding medium on dry ice. Cryosections were cut at 16 μm using a MICROM 500M Cryostat. For co-staining, sections were washed with PBSTw and blocked for 30 min with 2% sheep serum. Polyclonal rabbit anti-Pax2 (Covance, PRB-276P) was used in a 1:250 dilution, and polyclonal rabbit anti-Sox9 (Chemicon, AB5535) in a 1:500 dilution. Sections were incubated with primary antibody overnight at 4°C, rinsed with PBSTw, incubated with anti-rabbit TRITC (1:300 dilution) for 2–3 hr at room temperature, and rinsed with PBSTw. Rhodamine peanut agglutinin (PNA) (Vector Laboratories, RL-1072) was incubated at room temperature (1:400 dilution) for three hours, after blocking, then rinsed with PBSTw. ProLong Gold, antifade reagent (Invitrogen) was used for mounting. Images were taken on either an Olympus BX-51 upright light microscope with an Olympus DP70 camera, or a Zeiss LSM 510-META Laser Scanning Confocal Microscope mounted on a Zeiss Axiovert 100M inverted microscope using an argon laser. All green fluorescence shown in figures are images showing direct detection of fluorescence of eGFP from the *Hoxa11eGFP* allele.

Whole-Mount In Situ Hybridization

Embryos were treated as previously described (Huppert et al., 2005). Images were taken on a Leica MZ125 dissecting microscope with a Leica DFC480 camera.

ACKNOWLEDGMENTS

This research is supported (in part) by the National Institutes of Health through the University of Michigan's Cancer Center Support Grant (5 P30 CA46592). We acknowledge Elizabeth

Hughes, Yun Yan Qu, Keith Childs, and Galina Gavrilina for preparation of gene-targeted mice and the Transgenic Animal Model Core of the University of Michigan's Biomedical Research Core Facilities. Core support was provided by The University of Michigan Cancer Center, NIH grant number CA46592, and the University of Michigan Center for Organogenesis. The authors gratefully acknowledge the Michigan Economic Development Corporation and the Michigan Technology Tri-Corridor for the support of this research program (Grant 085P1000815). D.W. was funded by NIH DK071929 and DK077045.

REFERENCES

Bunting M, Bernstein KE, Greer JM, Capecchi MR, Thomas KR. 1999. Targeting genes for self-excision in the germ line. Genes Dev 13:1524–1528.

Condie BG, Capecchi MR. 1994. Mice with targeted disruptions in the paralogous genes hoxa-3 and hoxd-3 reveal synergistic interactions. Nature 370:304–307.

Davis AP, Witte DP, Hsieh-Li HM, Potter SS, Capecchi MR. 1995. Absence of radius and ulna in mice lacking hoxa-11 and hoxd-11. Nature 375:791–795.

Fromental-Ramain C, Warot X, Lakkaraju S, Favier B, Haack H, Birling C, Dierich A, Doll e P, Chambon P. 1996. Specific and redundant functions of the paralogous Hoxa-9 and Hoxd-9 genes in forelimb and axial skeleton patterning. Development 122:461–472.

Gendron RL, Paradis H, Hsieh-Li HM, Lee DW, Potter SS, Markoff E. 1997. Abnormal uterine stromal and glandular function associated with maternal reproductive defects in Hoxa-11 null mice. Biol Reprod 56:1097–1105.

Haack H, Gruss P. 1993. The establishment of murine Hox-1 expression domains during patterning of the limb. Dev Biol 157:410–422.

Horan GS, Ramirez-Solis R, Featherstone MS, Wolgemuth DJ, Bradley A, Behringer RR. 1995. Compound mutants for the paralogous hoxa-4, hoxb-4, and hoxd-4 genes show more complete homeotic transformations and a dose-dependent increase in the number of vertebrae transformed. Genes Dev 9:1667–1677.

Hsieh-Li HM, Witte DP, Weinstein M, Branford W, Li H, Small K, Potter SS. 1995. Hoxa 11 structure, extensive antisense transcription, and function in male and female fertility. Development 121: 1373–1385.

Huppert SS, Ilagan MX, De Strooper B, Kopan R. 2005. Analysis of Notch function in presomitic mesoderm suggests a gamma-secretase-independent role for presenilins in somite differentiation. Dev Cell 8:677–688.

Langford KG, Shai SY, Howard TE, Kovac MJ, Overbeek PA, Bernstein KE. 1991. Transgenic mice demonstrate a testis-specific promoter for angiotensin-converting enzyme. J Biol Chem 266:15559–15562.

Mansour SL, Thomas KR, Capecchi MR. 1988. Disruption of the proto-oncogene int-2 in mouse embryo-derived stem cells: a general strategy for targeting mutations to non-selectable genes. Nature 336:348–352.

McIntyre DC, Rakshit S, Yallowitz AR, Loken L, Jeannotte L, Capecchi MR, Wellik DM. 2007. Hox patterning of the vertebrate rib cage. Development 134:2981–2989.

Muyrers JP, Zhang Y, Testa G, Stewart AF. 1999. Rapid modification of bacterial artificial chromosomes by ET-recombination. Nucleic Acids Res 27:1555–1557.

Muyrers JP, Zhang Y, Benes V, Testa G, Rientjes JM, Stewart AF. 2004. ET recombination: DNA engineering using homologous recombination in E. coli. Methods Mol Biol 256:107–121.

Nagy A, Rossant J, Nagy R, Abramow-Newerly W, Roder JC. 1993. Derivation of completely cell culture-derived mice from early-passage embryonic stem cells. Proc Natl Acad Sci U S A 90:8424–8428.

Osoegawa K, Tateno M, Woon PY, Frengen E, Mammoser AG, Catanese JJ, Hayashizaki Y, de Jong PJ. 2000. Bacterial artificial chromosome libraries for mouse sequencing and functional analysis. Genome Res 10:116–128.

Patterson LT, Pembaur M, Potter SS. 2001. Hoxa11 and Hoxd11 regulate branching morphogenesis of the ureteric bud in the developing kidney. Development 128:2153–2161.

Peichel CL, Prabhakaran B, Vogt TF. 1997. The mouse Ulnaless mutation deregulates posterior HoxD gene expression and alters appendicular patterning. Development 124:3481–3492.

Small KM, Potter SS. 1993. Homeotic transformations and limb defects in Hox A11 mutant mice. Genes Dev 7:2318–2328.

van den Akker E, Fromental-Ramain C, de Graaff W, Le Mouellic H, Brulet P, Chambon P, Deschamps J. 2001. Axial skeletal patterning in mice lacking all paralogous group 8 Hox genes. Development 128:1911–1921.

Warot X, Fromental-Ramain C, Fraulob V, Chambon P, Dolle P. 1997. Gene dosage-dependent effects of the Hoxa-13 and Hoxd-13 mutations on morphogenesis of the terminal parts of the digestive and urogenital tracts. Development 124:4781–4791.

Wellik DM. 2007. Hox patterning of the vertebrate axial skeleton. Dev Dyn 236: 2454–2463.

Wellik DM, Capecchi MR. 2003. Hox10 and Hox11 genes are required to globally pattern the mammalian skeleton. Science 301:363–367.

Wellik DM, Hawkes PJ, Capecchi MR. 2002. Hox11 paralogous genes are essential for metanephric kidney induction. Genes Dev 16:1423–1432.

Wong KH, Wintch HD, Capecchi MR. 2004. Hoxa11 regulates stromal cell death and proliferation during neonatal uterine development. Mol Endocrinol 18:184–193.